

AERODYNAMICS CHARACTERISTICS DEVELOPMENT OF TARUMANAGARA ECO-VEHICLE (MOBIL IRIT UNIVERSITAS TARUMANAGARA) USING CFD METHOD

Janssen Paolo Yorkie, Steven Darmawan dan Harto Tanujaya

Department of Mechanical Engineering, Universitas Tarumanagara

e-mail: jp.yorkie@yahoo.com, stevend@ft.untar.ac.id, hartotan@ft.untar.ac.id

Abstract: *Vehicles experience the forces of aerodynamics at various degrees and magnitude. The impact of aerodynamic must be considered because it affects the efficiency of the object. Because aerodynamic forces highly affect a vehicle's efficiency, improvement in aerodynamics characteristics will improve the vehicles efficiency. However, the aerodynamic characteristic involves vehicle profile, dimensions. Designers now have the option of using a CFD software to simulate and calculate the aerodynamic properties of an object before production. The 2 objects on this research are an improved version of Mobil Irit Universitas Tarumanagara body by modifying its length therefore reducing the angle of the body, the body is named 3a and 3b. CFD simulation of body 3a and 3b is used to determine whether the flow characteristic is improved by the length modification of the object, and will be done using ANSYS Workbench R1 Academics Version at 5 different inlet velocity (1,39 m/s; 2,78 m/s; 4,17 m/s; 5,56 m/s; and 12,5 m/s) and will use a 3D simulation with single phase fluid. Subject 3a has 42699 nodes 234941 elements, subject 3b has 49535 nodes 272509 elements. The result shows a reduction in wake size at the back of subject 3b, whereas wake size increased in subject 3a. The drag coefficient result in reduction on 3b and an increase in 3a.*

Keywords: *Aerodynamics, Drag coefficient, CFD*

INTRODUCTION

Aerodynamic effects are present on our daily basis and could be detrimental to safety. It also plays an important role in efficiency of vehicles which results in more or less emissions overall [1]. The shape of a vehicle effects the flow of air around its surface, and this flow will determine the characteristic forces that are present during motion [2]. Mobil Irit Universitas Tarumanagara is designed to compete in Eco vehicle competition hosted by Shell which encourage research development and interest in the vehicle industry, mainly the efficiency aspect, in hope that a net-zero emission vehicles will someday be the product by pushing teams to make their vehicles more efficient and using the research results to push towards vehicles that is more environmentally friendly in the near future [3].

Designing a vehicle that can meet those requirements is a very challenging since it is related to many aspect such as mechanical design, ergonomics and aerodynamics as well. While others aspect performance can be estimated easier with numerous test, aerodynamics performance need more engineering, cost and time resources. Mobil Irit Tarumanagara uses CFD method to provide aerodynamics analysis since CFD simulation which is readily available for use now with many software to choose from will help engineers design their work to be efficient and also more importantly and safe. The purpose of this research is to improve the geometry design of Mobil Irit Tarumanagara Vehicle, in order to reduce drag coefficient and therefore less drag forces acting on the object. This will result in better fuel efficiency, which will improve the chances of winning the eco Vehicle Competition by Shell.

The simulation will use SST $k-\omega$ as the viscous model, with other parameters such as fluid density, temperature, humidity, pressure, and velocity being constant. The SST $k-\omega$ is a function of two equation eddy-viscosity model and is regularly used to simulate on aerodynamic test subjects. $k-\omega$ function is known to be well suited for flow simulation in the viscous sub-layer.

RESEARCH METHODOLOGY

The study is done numerically using CFD simulation to subjected body, which is named 3a and 3b as shown in figure 1. These 2 models are improved model from the original model by Poppy et al [4], previous model number 3 [4] . The length is modified to decrease overall surface area in

body 3a, and increase the flow characteristic in body 3b. The simulation will be done at 5 different velocities, which can be represented by 5 different Reynolds Number. The Reynold number value is the same in both test subject at the same velocity because the inlet size is the same for both. The Reynolds Number values are (328,779.992; 657,559.844; 986,339.779; 1,315,117.69; 2,956,653.98 at 1.36; 2.78; 4.17; 5.56; and 12.5 m/s respectively). The meshing will include general mesh with medium smoothing, which produce 42,699 Nodes 234,941 Elements for subject 3a, and 49,535 Nodes 272,509 Elements for subject 3b as shown in figure 2.

Boundary Condition

The boundary conditions in this simulation are:

- Fluid type: Air (single phase), Steady State
- Viscous Model: SST K- ω
- Initial pressure: 1 atm
- Initial temperature: 300K
- Relative humidity: 70%
- Fluid density: 1.16576 kg/m³
- Inlet velocity: 1.39 m/s; 2.78 m/s; 4.17 m/s; 5.56 m/s; 12.5 m/s
- Mesh smoothing: Medium

Test Model

The Following is the model used in this research.

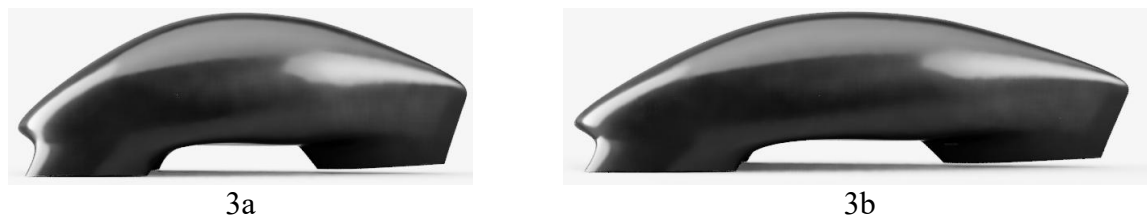


Figure 1. 3d rendering of subject 3a and 3b

The specification of the model can be seen on the table below:

Table 1. Subject specification

No.	Item	Body 3a	Body 3b
1	Surface Area	4.645 x 10 ⁶ mm ³	5.828 x 10 ⁶ mm ³
2	Volume	6.035 x 10 ⁸ mm ³	7.711 x 10 ⁸ mm ³
3	Length	2,553.3 mm	3,262.55 mm
4	Width	906.069 mm	906.069 mm
5	Height	805.248 mm	805.248 mm

Computational Domain and Mesh

The computational domain dimensions are the following. 3a has an inlet with a width of 4,9m and height of 3,1m for both 3a and 3b. The length for 3a is 12,5m and for 3b is 13,2m. The mesh in this research uses tetrahedral mesh, with medium smoothing. This configuration is chosen based on the mesh dependency analysis in “CFD Analysis of flow around AF1300a Cylinder Model at Reynolds Number Variation” by J. Paolo [5]. The following figure 2 shows the computational domain and mesh for subject model 3a and 3b. The mesh configuration result in 3a having 42699 nodes 234941 elements, and 3b having 49535 nodes 272509 elements.

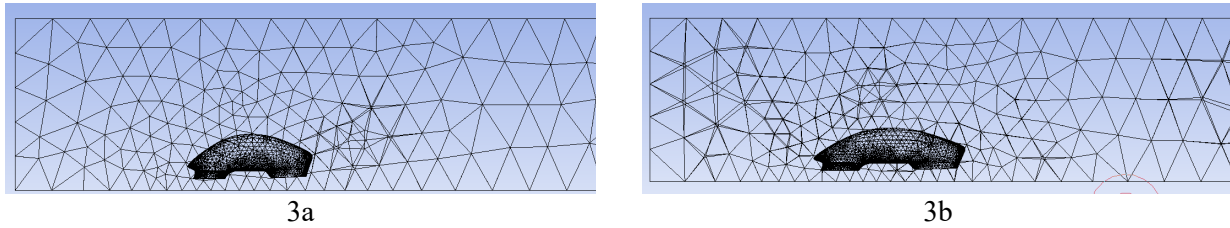


Figure 2. 3a and 3b Mesh

RESULTS AND DISCUSSION

Firstly, convert the inlet velocity into inlet Reynolds Number. This way another researcher could replicate the simulation or lab experiment with different inlet size by adjusting the inlet velocity to get the same Reynolds Number Value. The formula for calculating Reynolds Number in a square shaped duct is as the following [6].

$$Re = \frac{\rho \times D_h \times V}{\mu} \quad (1)$$

$$D_h = \frac{4 \times A}{U} \quad (2)$$

Where:

- Re: Reynolds Number
- ρ : Fluid Density (kg/m^3)
- D_h : Pipe Diameter or Hydraulic Diameter (m)
- V : Fluid flow velocity (m/s)
- μ : Dynamic viscosity of fluid (kg/m-s)
- D : Hydraulic Diameter (m)
- A : Area of the Duct (m^2)
- U : Wetted Perimeter of the Duct (m)

Table 2. Test Reynolds number at each velocity

No.	Velocity (m/s)	Reynolds Number
1	1.39	328779.922
2	2.78	657559.844
3	4.17	986339.766
4	5.56	1315117.69
5	12.5	2956653.98

General governing equation of the model including the SST $k-\omega$ turbulence model which are used are follows [7][8][9]:

$$P_1 + \frac{1}{2}\rho v_1^2 + \rho g h_1 = P_2 + \frac{1}{2}\rho v_2^2 + \rho g h_2 \quad (3)$$

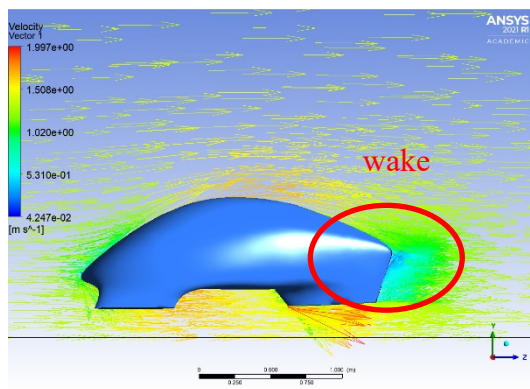
$$F_D = \frac{1}{2}C_D A \rho v^2 \quad (4)$$

$$\frac{\partial \rho K}{\partial t} + \frac{\partial}{\partial x_j} (\rho v_j K) = \frac{\partial}{\partial x_j} \left[(\mu_L + \sigma_K \mu_T) \frac{\partial}{\partial x_j} \right] + T_{ij}^F S_{ij} - \beta^* \rho \omega K \quad (5)$$

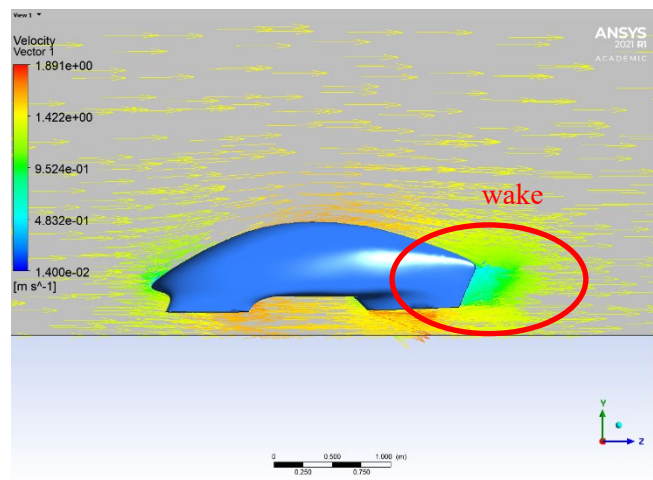
$$\begin{aligned} \frac{\partial \rho \omega}{\partial t} + \frac{\partial}{\partial x_j} (\rho v_j \omega) &= \frac{\partial}{\partial x_j} \left[(\mu_L + \sigma_\omega \mu_T) \frac{\partial \omega}{\partial x_j} \right] + \frac{C_w \rho}{\mu_T} T_{ij}^F S_{ij} - \beta \rho \omega^2 \\ &+ 2(1 - f_1) \frac{\rho \sigma_{\omega 2}}{\omega} \frac{\partial K}{\partial x_j} \frac{\partial \omega}{\partial x_j} \end{aligned} \quad (6)$$

Z-velocity and Pressure-contours and vectors

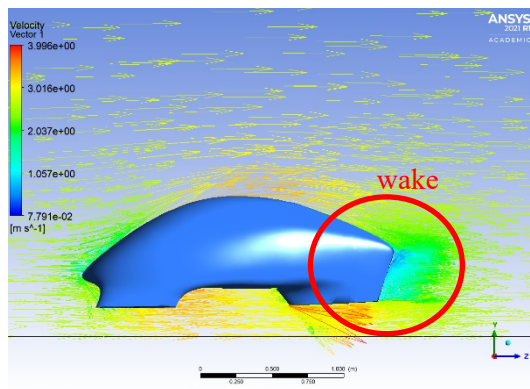
Velocity resulted by the subjected geometry is presented by Z-velocity and pressure contour, considering that the geometry is differentiate only on side part of the model.



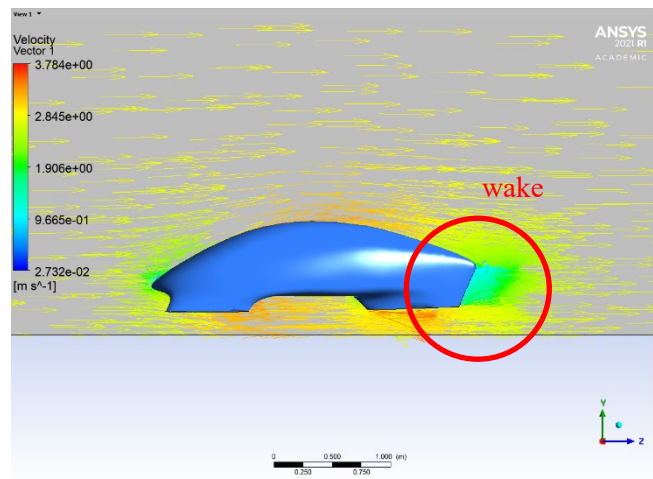
3a at Re = 328779,922



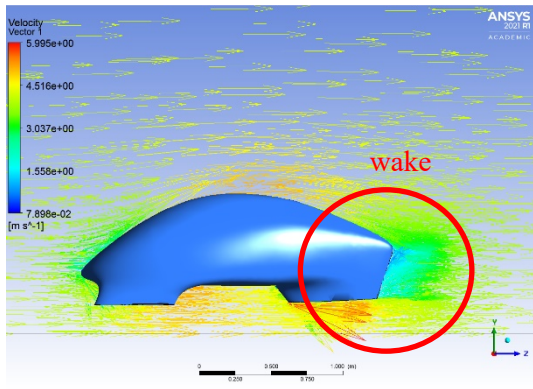
3b at Re = 328779,922



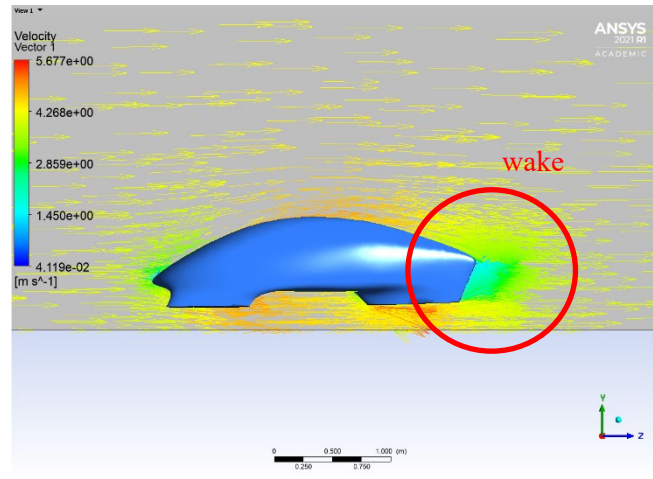
3a at Re = 657559,844



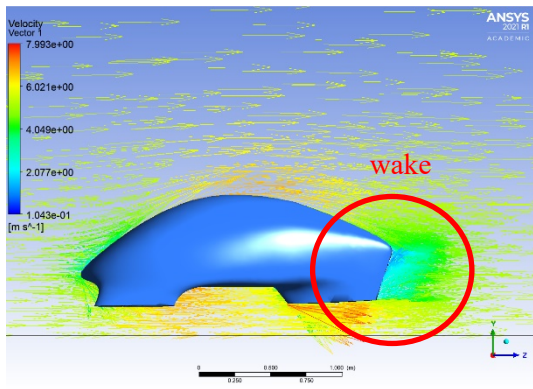
3b at Re = 657559,844



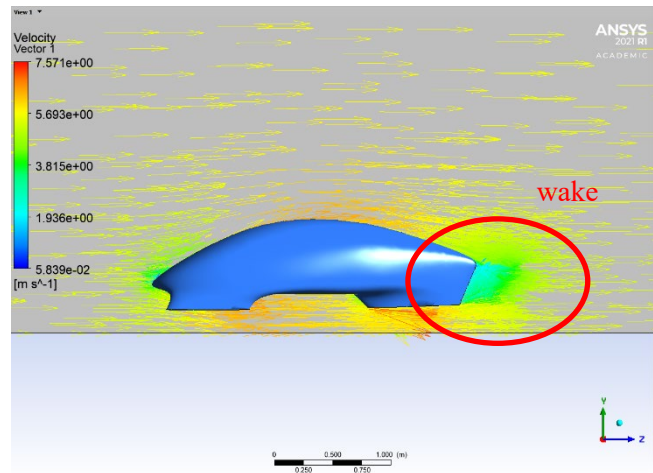
3a at Re = 986339,766



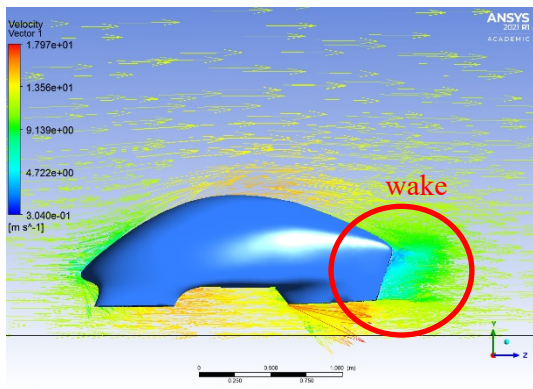
3b at Re = 986339,766



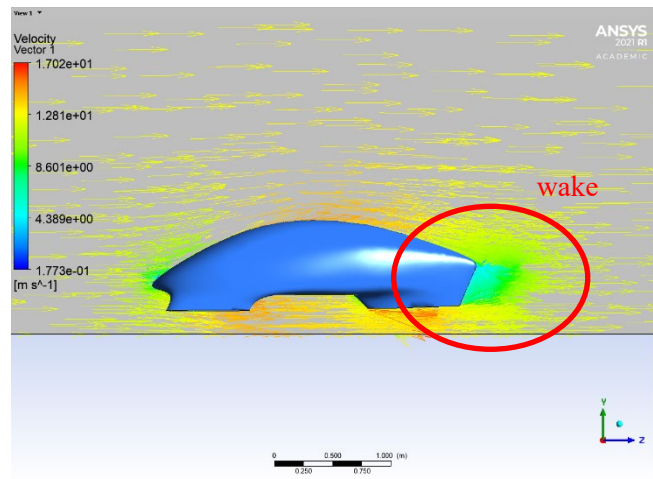
3a at Re = 1315117,69



3b at Re = 1315117,69



3a at Re = 2956653,98

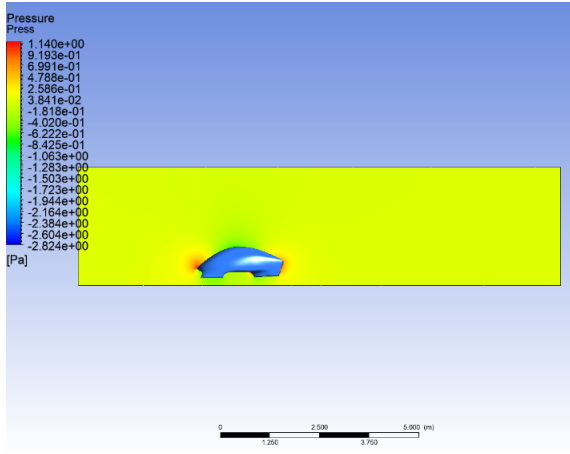


3b at Re = 2956653,98

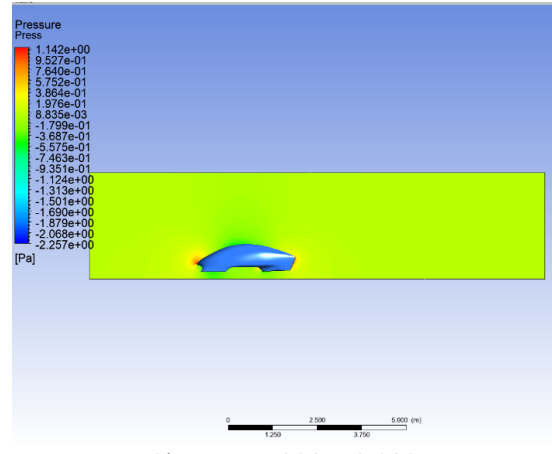
Figure 3. Z Velocity vector

Table 3. Velocity data

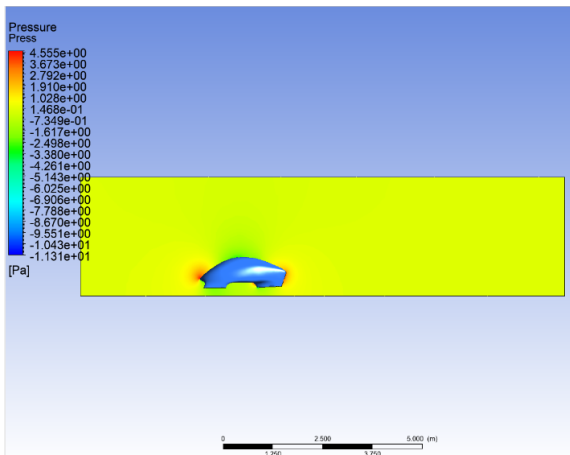
No.	Reynolds Number	3a		3b	
		Max Z Velocity (m/s)	Min Z Velocity (m/s)	Max Z Velocity (m/s)	Min Z Velocity (m/s)
1	328779.922	2.01767	0.0131363	1.89092	0.0140438
2	657559.844	4.03851	0.0278108	3.78413	0.0265916
3	986339.766	6.05945	0.042369	5.67744	0.0396391
4	1315117.69	8.08043	0.0574736	7.57083	0.0600795
5	2956653.98	18.1721	0.137595	17.0248	0.176471



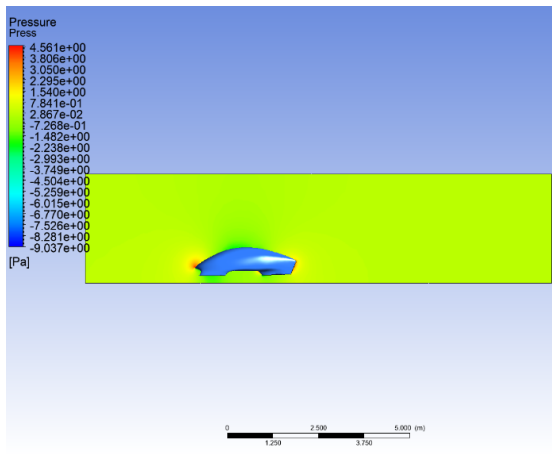
3a at Re = 328779,922



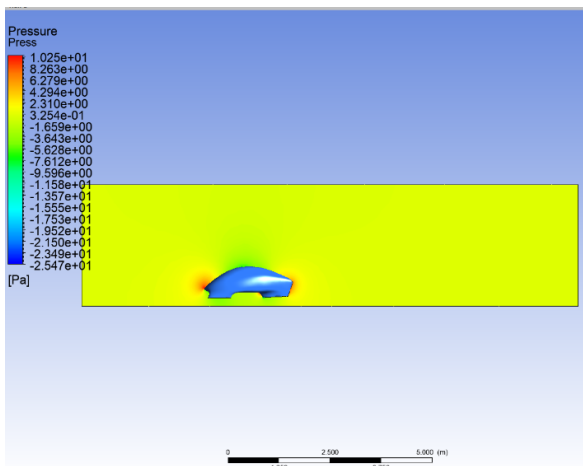
3b at Re = 328779,922



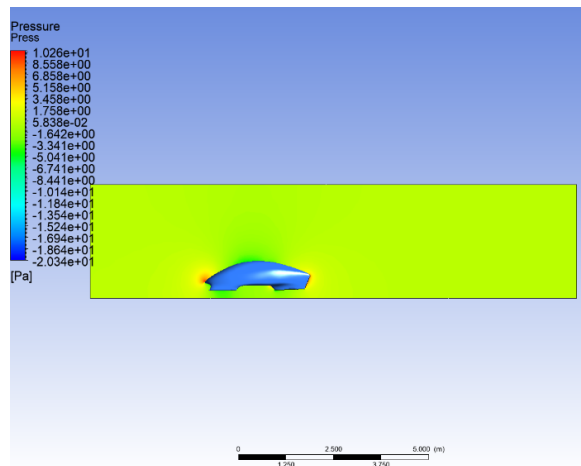
3a at Re = 657559,844



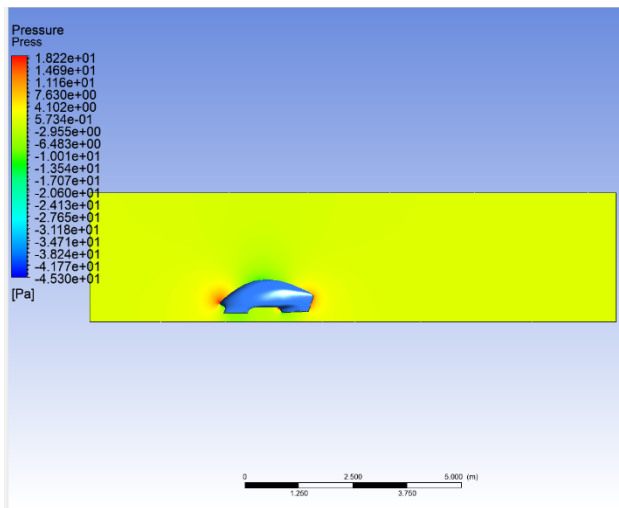
3b at Re = 657559,844



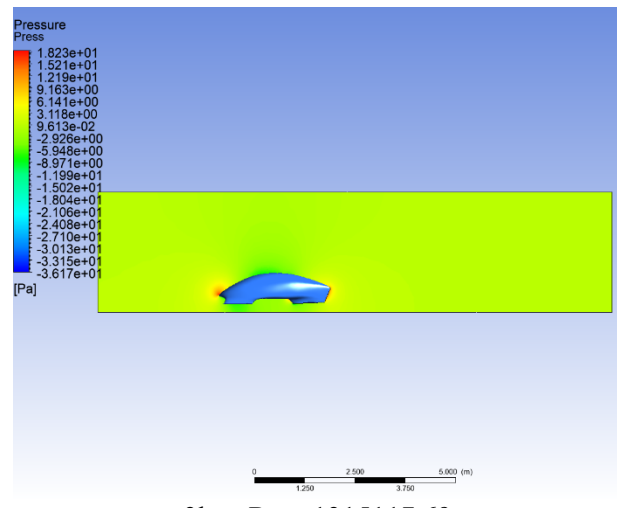
3a at Re = 986339,766



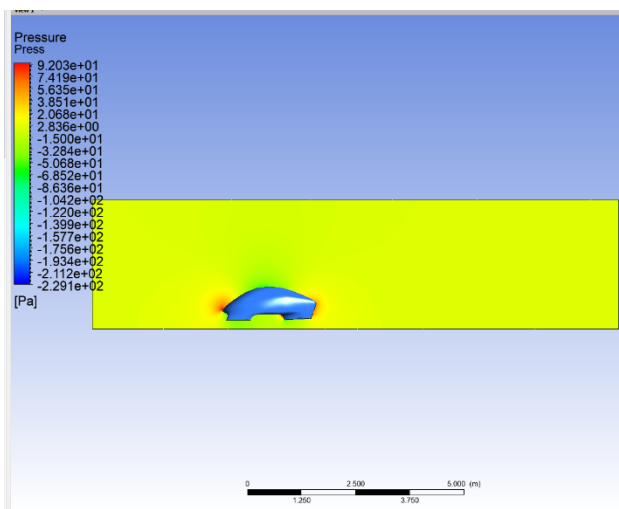
3b at Re = 986339,766



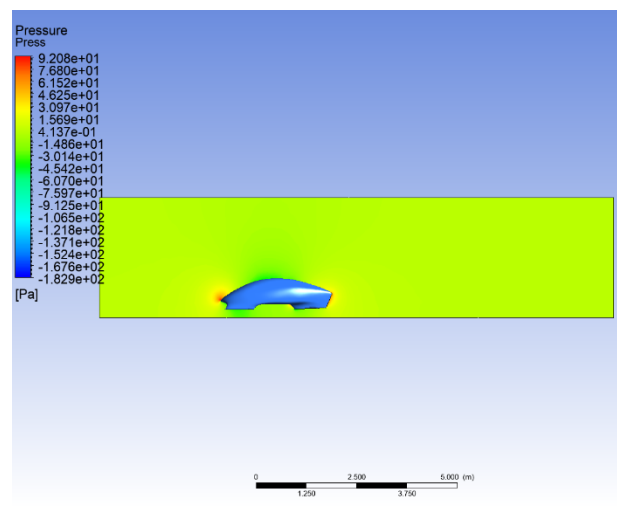
3a at Re = 1315117,69



3b at Re = 1315117,69



3a at Re = 2956653,98



3b at Re = 2956653,98

Figure 4. Pressure Contour

Figure 3 and figure 4 show simulation results that is represented by z-velocity and pressure. For all the simulation configuration, the flow is separated at the top of the model 3a as seen on figure 3, in the velocity vector we could see that subject 3a has a separation of flow, whereas in 3b simulation the flow stays attached to the object in every test. This is because the wind-shield angle of the body is too steep in subject 3a [10], making the flow of air more streamline on subject 3b than 3a. At the front of the object subject 3a has a larger velocity area than subject 3b. This result in a larger area of pressure difference as can be seen on the pressure simulation. At the back of the object, we could see the velocity area is also larger in 3a simulation than 3b, this result in 3a having a larger wake area, compared to 3b as can be seen on figure 4. Subject 3a will have a larger drag force acting on it as can be seen at the front and rear of the object on velocity simulation. A larger area of wake corresponds to a larger drag force and therefore a larger drag coefficient [11]. In subject 3b the wake area is significantly smaller due to the back area of the body that not as sharp as body 3a, therefore will have a smaller drag force.

At the back of the object, we could also see a higher velocity in the wake area on subject 3a, hinted by blue. According to Bernoulli principle of high fluid velocity = low pressure [8], this means the pressure at the rear of subject 3a will be lower than that of subject 3b which in accordance to better performance. Lower pressure at the rear of the object to be high as a low pressure will induce drag. The flow of air on the wake area behind the object actually form a curl towards the low-pressure

area called vortices or vortex, it is not visible because the vectors are on a straight line. This happens whenever the laminar flow of air is no longer strong enough to support its own flow [12], resulting in the air collapsing into the low pressure region and is an indicator of turbulent flow.

Table 4. Pressure data

No.	Reynolds Number	3a		3b	
		Max Pressure (Pa)	Min Pressure (Pa)	Max Pressure (Pa)	Min Pressure (Pa)
1	328779.922	1.15952	-2.82441	1.15868	-2.25653
2	657559.844	4.63515	-11.3147	4.63006	-9.03676
3	986339.766	10.4277	-25.4714	10.4123	-20.3404
4	1315117.69	18.5359	-45.2952	18.5045	-36.1711
5	2956653.98	93.6546	-229.077	93.4684	-182.918

Table 5. Coefficient of lift

No.	Reynolds Number	Body 3a	Body 3b
1	328779.922	0.1459	0.1343
2	657559.844	0.5801	0.5328
3	986339.766	1.3026	1.1933
4	1315117.69	2.3135	2.1191
5	2956653.98	11.672	10.688

Table 6. Drag coefficient on vehicle body 3a and 3b at varied Reynolds number

No.	Reynolds Number	Body 3a	Body 3b
1	328779.922	0.0425	0.0306
2	657559.844	0.1675	0.1201
3	986339.766	0.3747	0.2682
4	1315117.69	0.6641	0.4748
5	2956653.98	3.3361	2.3802

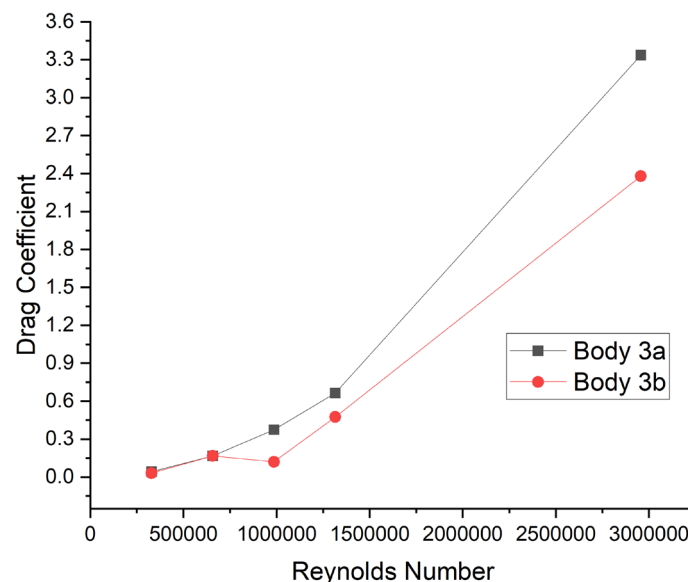


Figure 5. Drag coefficient in Vehicle body 3a and 3b at varied Reynolds number

The coefficient of drag from CFD simulation provided in table 6. The vehicle with body 3a and 3b will experience a bigger drag at higher Reynolds number which governed by equation (4). It is also clearly seen how the coefficient of drag behave on Reynolds number. The drag result comparing subject 3a and 3b confirms the analysis of drag forces and drag coefficient due to streamline profile, and wake size area. The result shows subject 3b has a lower coefficient of drag

than subject 3a in every velocity or Reynolds number. This phenomenon also confirmed on figure 5 which show that the drag coefficient is higher at higher velocity on body 3a and body 3b, and the body 3b has a lower drag coefficient than body 3a as the velocity is increased. This results also show body 3b with inclination at the back of the vehicle body not as sharp as body 3a gain better aerodynamics performance.

CONCLUSIONS

CFD simulation is conducted to 2 new body of Mobil Irit Tarumanagara Eco Vehicle which also compared to the previous body design. The model is subjected to several boundary condition which is based on specific requirements. The Reynolds number is set to $Re = 328779,922$; $Re = 657559,844$; $Re = 986339,766$; $Re = 1315117,69$; $Re = 2956653,98$. Based on the CFD simulation, Model 3b show better performance than the 3a which indicated with smaller wake at the back of the body as well as the lower pressure around the body. Model 3a also show lower coefficient of drag on Reynolds number variation. Model 3b is chosen to be developed in future research.

REFERENCES

- [1] M. N. Sudin, M. A. Abdullah, S. A. Shamsuddin, F. R. Ramli, and M. M. Tahir, "Review of research on vehicles aerodynamic drag reduction methods," *Int. J. Mech. Mechatronics Eng.*, vol. 14, no. 2, pp. 35–47, 2014.
- [2] J. Katz, "Aerodynamics of race cars," *Annu. Rev. Fluid Mech.*, vol. 38, pp. 27–63, 2006, doi: 10.1146/annurev.fluid.38.050304.092016.
- [3] SHELL, "Shell ECO MARATHON OFFICIAL RULES 2021 Chapter 1," vol. 1, no. 1, p. 59, 2020.
- [4] P. Kesuma, S. Darmawan, and A. Halim, "Aerodynamics analysis of mobil irit tarumanagara using CFD method," *IOP Conf. Ser. Mater. Sci. Eng.*, vol. 1007, no. 1, 2020, doi: 10.1088/1757-899X/1007/1/012032.
- [5] J. Paolo, "CFD Analysis of Flow Around AF1300a Cylinder Model at Reynolds Number Variation," *Publ. Pending*, no. 1.
- [6] MHRD, "Module 4 : Lecture 1 COMPRESSIBLE FLOWS (Fundamental Aspects: Part - I)," *NPTel - Mech. - Princ. Fluid Dyn.*, pp. 1–57, [Online]. Available: <https://nptel.ac.in/courses/101103004/pdf/mod4.pdf>.
- [7] S. Ideen, "Aerodynamic Basics," pp. 0–234, 2018, [Online]. Available: <https://denmachines.com/2017/07/26/aerodynamic-basics/>.
- [8] J. M. C. Yunus A. Cengel, *Fluid Mechanics*. Pennsylvania, 1377.
- [9] K.-J. Bathe, *Computational fluid and solid mechanics 2003[Recurso electrónico]:] proceedings, Second MIT Conference on Computational Fluid and Solid Mechanics, June 17-20, 2003*. 2003.
- [10] J. Wang, H. Li, Y. Liu, T. Liu, and H. Gao, "Aerodynamic research of a racing car based on wind tunnel test and computational fluid dynamics," *MATEC Web Conf.*, vol. 153, pp. 1–5, 2018, doi: 10.1051/mateconf/201815304011.
- [11] R. Merrick and G. Bitsuamlak, "Control of flow around a circular cylinder by the use of surface roughness," pp. 1–15, 2008.
- [12] S. H. S.P and W. A. Widodo, "Karakteristik Wake Area Akibat Efek Penggunaan Vortex Generator di Belakang Wing Airfoil Naca 43018," *J. Penelit.*, vol. 4, no. 1, pp. 55–63, 2019, doi: 10.46491/jp.v4e1.287.55-63.